

RSC Advances



This is an *Accepted Manuscript*, which has been through the Royal Society of Chemistry peer review process and has been accepted for publication.

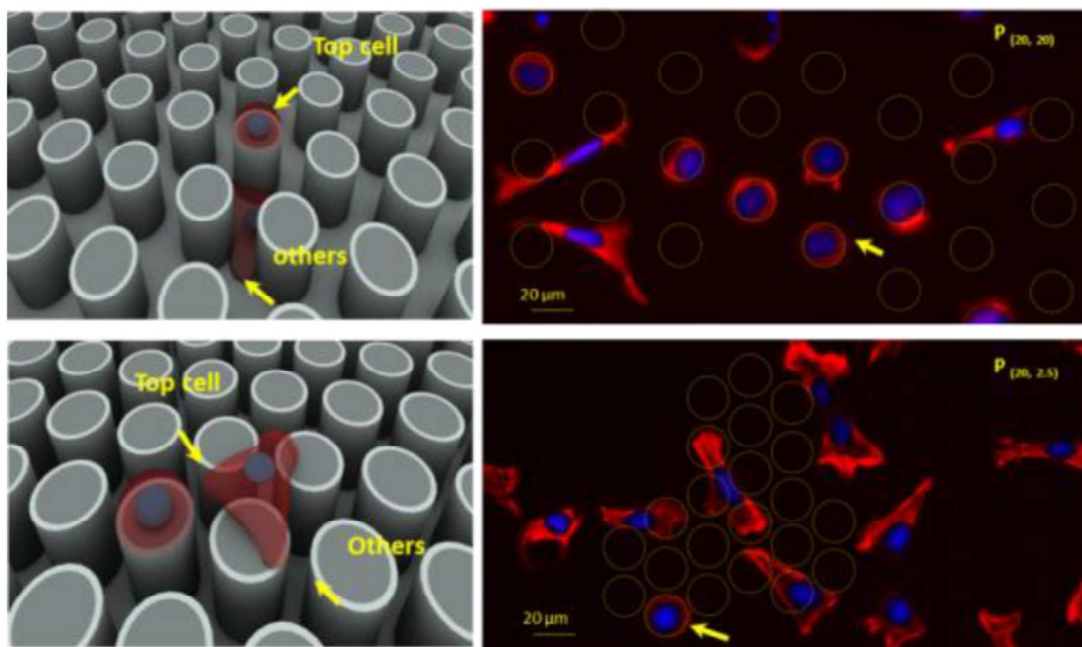
Accepted Manuscripts are published online shortly after acceptance, before technical editing, formatting and proof reading. Using this free service, authors can make their results available to the community, in citable form, before we publish the edited article. This *Accepted Manuscript* will be replaced by the edited, formatted and paginated article as soon as this is available.

You can find more information about *Accepted Manuscripts* in the [Information for Authors](#).

Please note that technical editing may introduce minor changes to the text and/or graphics, which may alter content. The journal's standard [Terms & Conditions](#) and the [Ethical guidelines](#) still apply. In no event shall the Royal Society of Chemistry be held responsible for any errors or omissions in this *Accepted Manuscript* or any consequences arising from the use of any information it contains.

Graphical Abstract

Micro pillar topographies can greatly influence the individual hepatic stellate cell behaviors, being triggered by a minimum interfacial energy.



Full Papers

Regulating Cell Behaviors on Micropillar Topography Affected by Interfacial Energy

Xinghua Gao¹, Yeung Yeung Chau^{2,ξ}, Jiao Xie⁵, Jun Wan¹, Yanxiao Ren⁴, Jianhua Qin^{3*}, Weijia Wen^{1,2,4,5*}

¹ *Biomedical Research Institute, Shenzhen Peking University - The Hong Kong University of Science and Technology Medical Center, Shenzhen, China*

² *Department of Physics, The Hong Kong University of Science and Technology, Clear Water Bay, Kowloon, Hong Kong*

³ *Key Laboratory of Separation Science for Analytical Chemistry, Dalian Institute of Chemical Physics, Chinese Academy of Sciences, Dalian, China*

⁴ *The Hong Kong University of Science and Technology Shenzhen Research Institute, Shenzhen, China*

⁵ *Soft Matter and Interdisciplinary Research Institute, College of Physics, Chongqing University, Chongqing, China*

^ξ *This author contributed equally to this work and should be considered as co-first author.*

** Correspondences:*

Prof. Weijia Wen, E-mail: phwen@ust.hk, Tel: +852-23587979

Prof. Jianhua Qin, E-mail: jhqin@dicp.ac.cn, Tel: +86-41184379650

Abstract

Micro/sub-micro substrate topography plays an important role in cell morphology and function. By localizing the individual hepatic stellate cell on different micropillar topographies, we found that the cell morphology was thus greatly influenced due to the cell location. As a simple physical modeling showed, the morphological response of cells to micropillar topography can be triggered by a minimum interfacial energy. In particular, the established topography with the spacing of 2.5 μm and the pillar diameter of 5 μm was found to be able to change the expression of E-cadherin and α -smooth muscle actin. It suggested that the size of the established topography might be closely related to cell epithelial-mesenchymal transition. This study has potential significance in mimicking the size of Disse's space in pathological conditions and advanced the understanding of the physical mechanisms of liver fibrosis and cirrhosis.

1. Introduction

The complex cellular microenvironment in which cells reside and survive is a dynamic system *in vivo*, and plays an essential role in cell morphology and function [1]. Cells can respond to various environmental signals, which are categorized into biochemical cues or biophysical cues. These cues are mainly provided by the extracellular matrix (ECM), which acts as a cellular scaffold and exists as the primary extracellular component of tissues [2]. The ECM is composed of proteins and polysaccharides with structural widths and lengths in the micro and nanometer scales, providing biophysical structures of regular configuration and biochemical support to the surrounding cells [3]. The ECM is especially known to its close association with the physiological and pathological conditions *in vivo*, such as tumor and fibrosis [4, 5].

While the biochemical cues, such as small molecules, surrounding cells, and proteins have long been appreciated, attention has only recently been drawn to the biophysical cues, such as the mechanical properties [6], matrix elasticity [7, 8] and topography of the substrates [2, 9-27]. Among the biophysical cues, the substrate topography generates variety of geometrically-defined, three-dimensional (3D) physical cues of the micron and sub-micron scales; it is well known in influencing the cellular adhesion, spreading, proliferation and other functions via the interactions between cells and the substrate. The studies on cell response to substrate topography were mainly focused on the investigation of the cell morphology and function on various types of substrate topographies, including pillars [9, 10], wells, grooves [11], protrusions [12, 13] and other anisotropic geometries [14]. In particular, cell adhesion and the formation of cell morphology on the topographic substrate are the initial and primary steps for guiding cell spreading and other functions. For instance, the sizes of micro pillars, such as the aspect ratios and pitch were shown to affect cell morphology and spreading. While the cells would adhere on the top of isotropic micro patterns, of which the size is compatible with the cells [15], cell polarity and the direction of cell

migration would be restricted on the anisotropic micro patterns, such as teardrop and ratchet [16, 17]. Furthermore, more evidences suggest that the topographies of micro- or nanoscales could promote and facilitate self-renewal and proliferation of stem cells [18]. Some specific topography could also enhance and direct stem cell differentiation, such as neuronal differentiation of neural stem cells (NSCs) [19, 20], mesenchymal stem cells (MSCs) [21, 22] and embryonic stem cells (ESCs) [23] on grooves with different aspect ratios, osteogenic differentiation of MSCs on nanoscale protrusions with a specially established dimension [24, 25].

Overall, cell morphology, spreading and other cellular function largely depend on the cell type, the geometry and dimension of the substrate topography. However, only a few cell types and substrate topography have been studied to date. The influence of substrate topography on cell behaviors with respect to morphology and functions calls for further exemplification. More systematic studies on other cell types apart from stem cells, such as tissue cells need to be conducted to demonstrate the cell behaviors and its biological mechanism guiding cell response to substrate topography. Analysis of the cell responses to different topographical cues, over multiple temporal and spatial scales, is central to the understanding of various main biological functions.

In this study, the hepatic stellate cells (HSCs) that lie in the Disse's space between parenchymal cells and sinusoidal endothelial cells of the hepatic lobule have been considered. These cells *in vivo* were related to various kinds of liver disease and showed obvious size-dependent properties in ECM. Therefore, the individual HSC behaviors in response to different size of micropillar topography have been demonstrated. The results showed that the established topography could influence cell morphology and expression of protein related to cell epithelial-mesenchymal transition (EMT). In addition, as a simple physical modeling showed, the morphological response of cells to micropillar topography can be triggered by a minimum interfacial energy.

2. Materials and methods

2.1 Fabrication of micropillar substrate topography

Micropillar substrate topographies were fabricated on silicon wafers by photolithographic methods, the process flow of the fabrication for the patterned surface was showed in Fig.1-A. After UV exposure by contact aligner (SUSS Microtec MA6) and developing the pattern on the wafer, we exposed bare silicon by etching the oxide layer not covered by the pattern by STS AOE Etcher, then undergone deep reactive ion etching (Surface Technology Systems, ICP DRIE) to generate vertical walls. The photoresist layer had been removed by plasma cleaning process (PS210 Photo Resist Asher), and the remnant oxide layer has been removed by oxide etcher. Thereafter, the patterned samples had undergone piranha cleaning process to remove all contaminants.

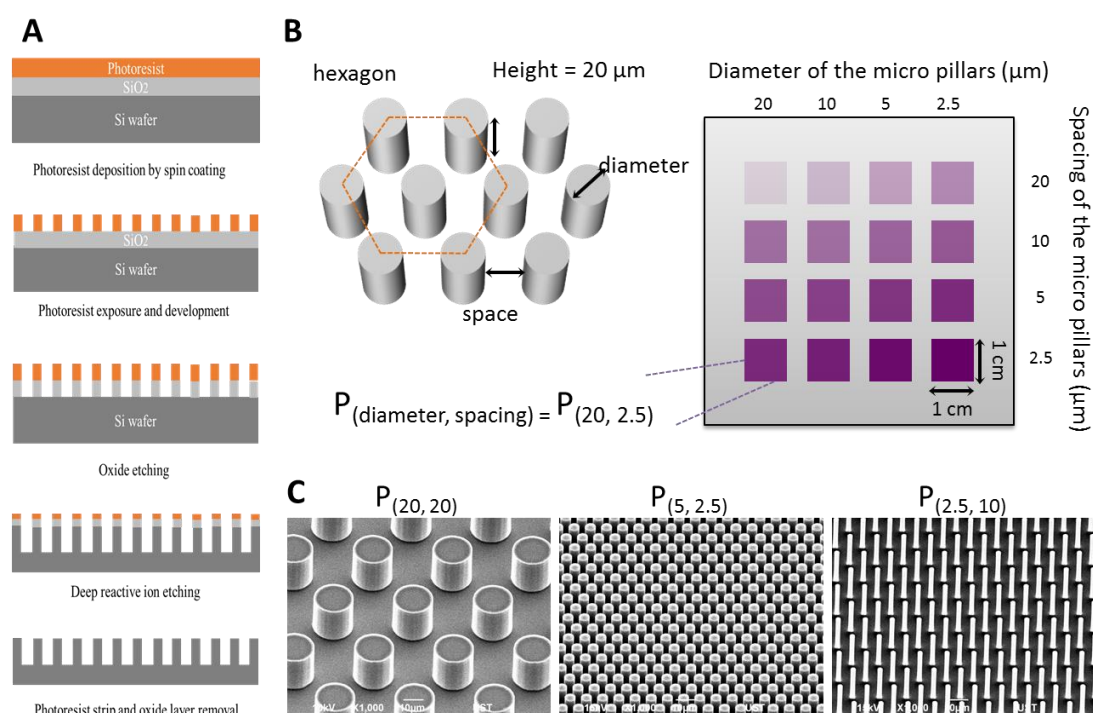


Figure 1. Micro pillar silicon substrate fabrication and characterization. A: the processes flow of micro pillar fabrication; B: Top view of the micro pillar substrate and 16 different micro pillar substrate groups; C: The SEM images of micro-pillars of different diameters and spacing used in the experiments, the x-axis indicates the

diameter of the micro pillars, and y-axis shows the side-to-side spacing between the adjacent micro-pillars.

2.2 Cell culture and EMT induction

A human hepatic stellate cell line, LX-2, was used in this study. The cells were maintained in Dulbecco's Modified Eagle's Medium with 4500 mg/L glucose (HG-DMEM), 10% fetal bovine serum (FBS), 100U/mL penicillin, 100 μ g/mL streptomycin at 37 °C in a humidified atmosphere, containing 95% air and 5% CO₂. LX-2 cells were seeded on the micropillar and flat silicon substrate at a density of 1500 cells/ cm² and incubated for various periods (1 day for cell morphology and migration or 3 days for expression of protein related to cell EMT). In particular, for the cell EMT assay, the transforming growth factor- β 1 (TGF- β 1) as drug inducer was added in the culture medium with 10 ng/ ml. After cell adherence in a culture dish about 24h, cells were exposed to the inducer medium for 48h and then detected. The HG-DMEM, FBS, penicillin and streptomycin were purchased from GIBCO, Invitrogen. The TGF- β 1 was obtained from R&D Systems, Minneapolis, MN, USA.

2.3 Cell fixation and staining

Expression of E-cadherin (E-cad) and α -smooth muscle actin (α -SMA) in LX-2 cells was performed by immunofluorescent assay. After cell treatment for 48 h, LX-2 cells on the micropillar and flat substrate were washed three times in PBS and fixed in 4% paraformaldehyde for 20 min at room temperature. For only α -SMA staining, an extra step, cells treated by 0.1% Triton X-100 was needed. After being washed by PBS, cells were blocked with goat serum for 1 h to decrease nonspecific hybridization. And then cells were incubated with anti-human E-cadherin or anti-human α -SMA primary antibody at a 1:100 dilution overnight, respectively. And next, cells were washed by PBS solution, and then incubated with the secondary antibody. The cell nucleus was stained by DAPI. After washing PBS sufficiently, the fluorescent images were obtained by the fluorescent microscope. F-actin for cell morphology was stained with Alexa Fluor 488 Phalloidin according to the reagent for manual operation. The

primary antibodies were obtained from R&D Systems, Minneapolis, MN, USA. The secondary antibody was purchased from Sigma. The PBS, Triton X-100, DAPI and Alexa Fluor 488 Phalloidin were purchased from Life, Invitrogen.

2.4 Cell detection and assay

Cells were visualized using an Olympus fluorescence microscopy (Olympus IX 71, Japan). For immunofluorescence analysis, quantitation was performed by analyzing the area of the fluorescence using Image-Pro Plus 6.0 software (Media Cybernetics, Silver Spring, MD, USA). Statistical analysis of the data was performed by using a Student's t-test.

2.5 Simulation of cell interfacial energy

The simulation model was constructed by the program Surface Evolver (Version 2.70, Kenneth Brakke, Mathematics Department, Susquehanna University, Selinsgrove, PA, USA), an interactive program for modelling liquid surfaces under various forces and constraints. It treats cells as liquid droplets spreading on micro patterned surfaces. We modeled the evolution of the given objects governed by minimization of energy according to the method in Ref 28. In Surface Evolver methods, geometric elements consisting vertices, edges, facets and bodies were used to build the model. The surface refers to all the geometric elements of the model entity set with boundaries, constraints and forces. The total energy of a surface resulting from the surface tension and gravitational force is which the Evolver minimizes.

3. Results and discussion

3.1 Characterization of micro-pillar substrate topography

Micro pillar areas of 1 cm^2 were fabricated on silicon wafers of $400 \text{ }\mu\text{m}$ by photolithographic methods, regular hexagonal arrays of circular micro pillars of $20 \text{ }\mu\text{m}$ with high aspect ratios of 1:8, 1:4, 1:2 and 1:1 corresponding to the micro-post diameters of $2.5 \text{ }\mu\text{m}$, $5 \text{ }\mu\text{m}$, $10 \text{ }\mu\text{m}$ and $20 \text{ }\mu\text{m}$ respectively. Fig. 1-A shows the

process flow of the fabrication for the patterned surface. For easy reference, we used $P_{(\text{diameter, spacing})}$ to denote the different micro pillar groups. For instance, $P_{(20, 2.5)}$ refers to the pillar group of which the corresponding diameter and spacing are $20\mu\text{m}$ and $2.5\mu\text{m}$. Fig.1-C shows the SEM images of the micropillar substrate topography.

3.2 Effects of micropillar topography on individual cell morphology

In this study, the attachment of LX-2 cells with a low concentration to ensure individual cell assay on micropillars, with flat substrate as the control were evaluated after seeding the cells for 24h. LX-2 cells showed a good viability on the micro patterned substrate and the flat silicon substrate. More than 95% of cells lived for more than 3 days on both substrates. To analyze the cell morphology, the cell F-actin and nucleus were stained by phalloidin and DAPI, respectively. The fluorescence images are shown in Figure 2-A.

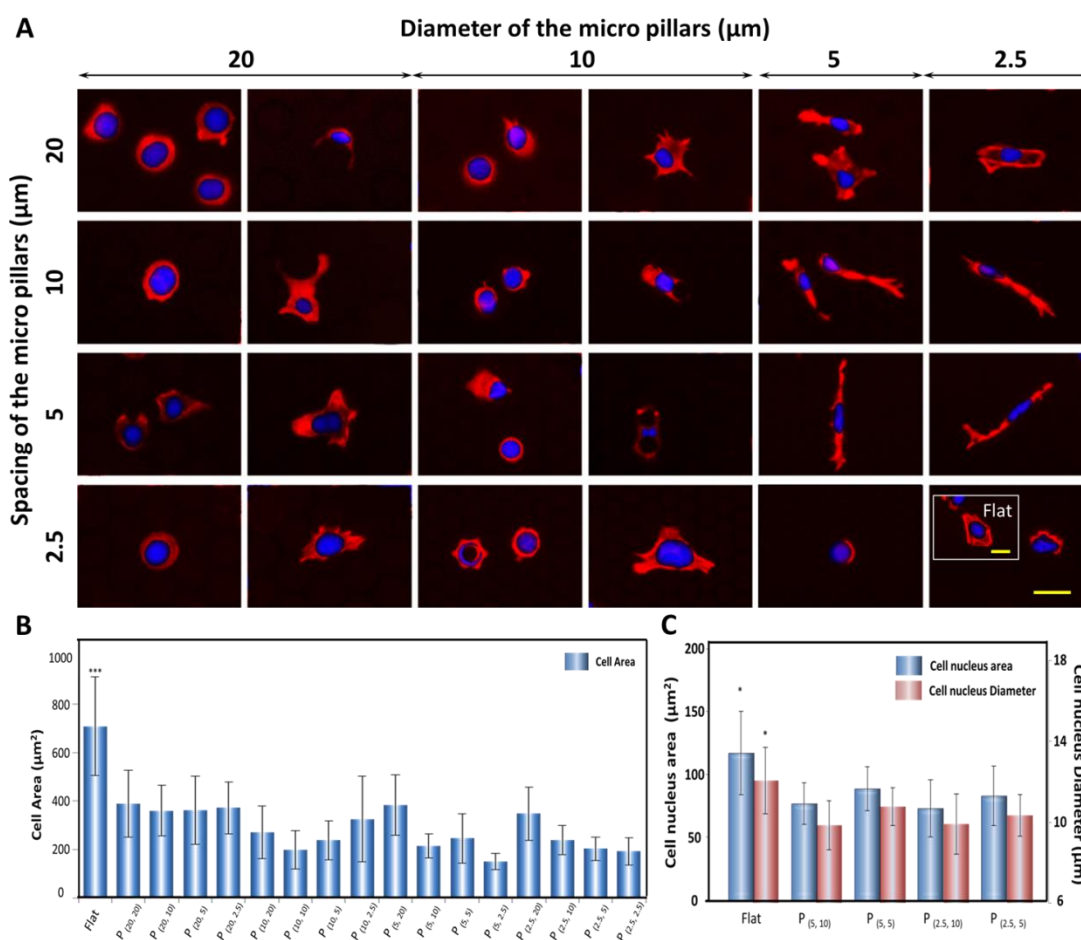


Figure 2. Individual LX-2 cell on the micro pillar substrate. A: Fluorescence images of individual cell morphology. The illustration was cell F-actin and nucleus staining on flat substrate. Red: F-actin; Blue: cell nucleus; bars = 20 μm . B: Cell area of different micropillar group and flat substrate. ***: $p < 0.005$; C: The areas and mean diameters of cell nucleus of P_(5, 10), P_(5, 5), P_(2.5, 10), P_(2.5, 5) and flat substrate. *: $p < 0.05$; n = 11.

We found that the cell morphology was closely related to the cell location, which was created by the diameter and spacing of micropillar. Generally, the size of the suspending mammalian cells was about 10 – 20 μm in diameter. So for the 20 μm spacing of micro-pillar, the individual cell could culture at the bottom of the gap between pillars [P_(20, 20) P_(10, 20) P_(5, 20) P_(2.5, 20)] or on the top of one pillar [P_(20, 20) P_(10, 20)]. For spacing of 10 μm and 5 μm , the cell location became complicated. The individual cell could either hang between the gap and adhere to several pillars [P_(20, 10) P_(10, 10) P_(5, 10) P_(2.5, 10) P_(20, 5) P_(10, 5) P_(5, 5) P_(2.5, 5)] or on the top of one single pillar [P_(20, 10) P_(10, 10) P_(20, 5) P_(10, 5)]. And with the spacing of 2.5 μm , the cell could adhere on the top of one pillar [P_(20, 2.5) P_(10, 2.5)] or several pillars [P_(20, 2.5) P_(10, 2.5) P_(5, 2.5) P_(2.5, 2.5)]. Overall, when the cell was on the top of one pillar, the cell shape adapted to the cross section of the micro pillar, i.e. circular with diameter similar to that of the pillar. On the other hand, when the cell was at the bottom of the gap between pillars, it could occupy the gap around the pillars. For larger pillars, the cell would be pushed out and the cell shape was abnormal [P_(20, 20) P_(10, 20)]. Otherwise, the cell shape was the same as on the flat substrate [P_(5, 20) P_(2.5, 20)]. When the cell was hanging between several pillars, there were obvious changes in the cell shape. In P_(5, 10), P_(5, 5), P_(2.5, 10) and P_(2.5, 5) groups, the cell shape was thinner and straighter than others. But in P_(20, 10), P_(20, 5), P_(10, 10) and P_(10, 5) groups, there was no obvious rule to follow. For the cells that adhered to several pillars, it was shown that if the cell was on the pillars with a little subsidence [P_(5, 2.5) P_(2.5, 2.5)], the cell shrank. Otherwise, the cell shape was the same as on the flat substrate [P_(20, 2.5) P_(10, 2.5)].

In addition, the area of individual cell, area of cell nucleus and mean diameter were calculated. It was found that the area of the cells on the micro pillar substrate decreased substantially compared to the flat substrate (as shown in Figure 2-B). This result was similar to the reported responses of the human umbilical vein endothelial cells (HUVECs) [29]. Some of cell morphology also resembled 3D cell culture in gel, and this change suggested that the micro pillar substrate might generate an approximate 3D gel-free environment for the individual cell survival. Furthermore, the area and mean diameter of cell nucleus decreased only in four different micro pillar groups [$P_{(5, 10)}$, $P_{(5, 5)}$, $P_{(2.5, 10)}$ and $P_{(2.5, 5)}$] compared to the flat substrate. The data are shown in Figure 2-C. In these micro pillar groups, the individual cell was thinner and straighter than it was on the flat substrate, and the shape of the cell nucleus also changed from round to elliptical, probably because the cell nucleus sat almost astride the narrow spacing between the pillars.

The “top cells”, refer to the cells for each staying right on the top of a single pillar, are commonly found on micro-pillars of 20 μm in diameter. The number of top cells has been counted and compared to the other cells. The percentage of top cell reached 73% and reduced with the decrease of the spacing, the reason for such reduction may be due to the narrower spacing, which enabled cell to adhere to on several pillars. More details are shown in Figure 3. The shape of the top cell adapted to the circular micro pillar. The area of top cell was $351.0 \pm 68.3 \mu\text{m}^2$ ($n = 16$) in $P_{(20, 20)}$ group, this value was very close to $314.1 \mu\text{m}^2$, which was the area of the cross section of the micro pillar. The value of the area of top cell had a small standard deviation, and it showed that the cell shape was more uniform than the others, such as the cell on flat substrate, with an area of $616.7 \pm 220.2 \mu\text{m}^2$ ($n = 16$). This unique phenomenon suggested that the cell can modulate itself to adapt to the topography of the substrates.

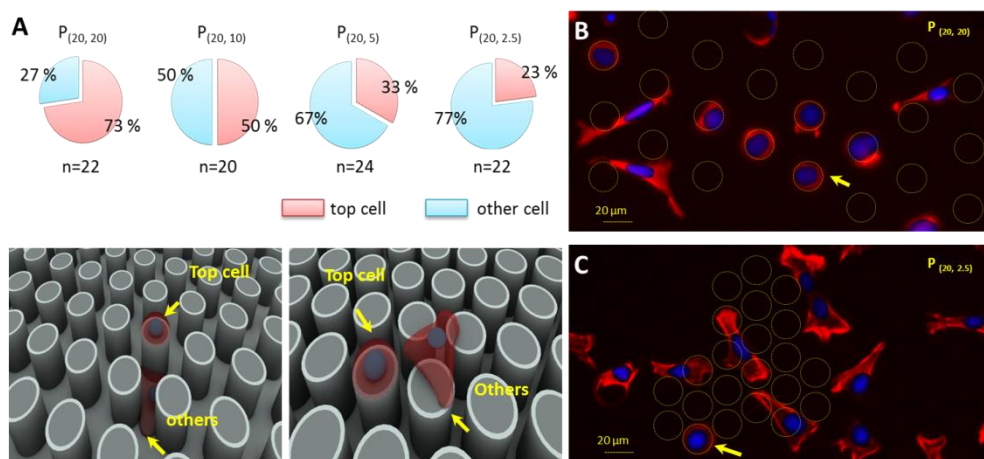


Figure 3. Individual cell morphology on the top of one micro pillar. A: the percentage of top cell in different micro pillar groups. B: Fluorescence image of individual cell morphology in $P_{(20,20)}$ group. C: Fluorescence image of individual cell morphology in $P_{(20,2.5)}$ group. Red: F-actin; Blue: cell nucleus. Scale bar = 20 μm .

3.2 Simulation of individual cell on different substrates

The changes of individual cell topography on the micro pillar substrate might be related to the surface energy of cell. So in this study, the program Surface Evolver (Version 2.70) has been used to construct a simple cell models. The Surface Evolver can be applied to create surfaces and volumes, impose energy boundary conditions and model the evolution of the given objects governed by minimization of surface energy. Cell models started as cuboids on substrate in this work. The cube was chosen as the starting configuration for simplicity and ease of simulation. The volume of cuboid was $8000 \mu\text{m}^3$, equal to volume of a sphere with diameter of 24.8 μm . This diameter was approximate to the diameter of normal suspending mammalian cells. In order to enhance the similarity between the cuboid and cell, one solid sphere of 10 μm diameter was inserted into cuboid as a non-spreading cell nucleus. This solid sphere as a fixed constraint prevents the infinite extensive spreading of the droplet on the flat substrate, but has no relevance on the bulged droplet since it doesn't touch its surface on the substrates with different pillars.

By considering small area on or just next to one micro pillar, we apply the Young's equation:

$$\gamma_{sl} = \gamma_{sv} - \gamma_{lv}(\cos \theta) \quad (1)$$

Where γ_{sl} is the solid-liquid interfacial energy, γ_{sv} is the solid-gas interfacial energy, γ_{lv} is the liquid-gas interfacial energy, θ is the Young's contact angle. In this simulation, the contact angle between the substrate and cuboid was set to 7° ; and the contact angle between cuboid and the surrounding area was set to 180° . The air-solid tension was considered to be neglected compared to liquid-solid tension and liquid-air tension. The liquid-air tension was set to be 1 in the following work. After add contact angle boundary conditions, the actual contact angle on the contact line was between 7° and 180° (non-spread contact angle on the non-wet substrate). These boundary conditions of the contact angle were the same as that in Ref. 28. Then the water-solid and interfacial energy could be calculated which reaches minimum when the system was equilibrium.

Four different initial conditions have been simulated: individual cell on the flat substrate, individual cell on the top of one micro pillar, individual cell beside one pillar and individual cell between two micro pillars. All micropillars' diameters were $20 \mu\text{m}$. Cells were simulated similarly to water droplets, being defined with an initial condition, incompressible volume, surface tension, contact angles between the different interfaces and an impenetrable solid sphere mimicking the nucleus. During simulation, the size of nucleus and cell volume could be considered constant during cell spreading on the substrates. Different wet side constraints were added in four models, respectively.

Each iteration was considered to be an evolution step in this work. We initial refined the cubic with triangle mesh, and obtained these initial states in Figure 4 (A_1 , B_1 , C_1 and D_1). Then go iterations until reach its minimum energy state. Each iteration contains these three following steps: Firstly, the force of vertex as a function of

position is calculated by the gradient of the surface energy, which directs the vertex motion. Secondly, the force conformed to constraints move the vertices into the proper area where constraints allowed. Thirdly, the actual motion can be realized by using a global interaction scale factor. (Surface Evolver Manual Version 2.70: <http://www.susqu.edu/brakke/evolver/downloads/manual270.pdf>). After that, the model was refined the second time and go iterations until its final equilibrium configuration. At last, we got the equilibrium configuration we care as the cell morphology.

By minimizing the energy, the cell model evolved until it was stable. The results are shown in Figure 4 (A2, B2, C2, and D2). According to the simulation results, when the cell was on the flat substrate without wet side constraints, it flattened and adhered with a maximum area of adhesion at the minimum surface energy state. But when the micro pillar was introduced, the spreading of individual cell would be resisted and restricted, and the simulated surface area of cell was decreased. The simulated area of cell beside one pillar or cell between two micro pillars was reduced to 88% and 85%, respectively. This trend was similar to the experimental data. Notably, the top cell was also simulated by the same method of minimum surface energy. This simulation result matches well with the experimental data. The cell morphology was like a spherical crown with basal diameter similar to that of the pillar. The simulation demonstrated that the change of cell morphology was associated with the cell surface energy. The steady or equilibrium state of cell morphology was the minimum surface energy of the cell.

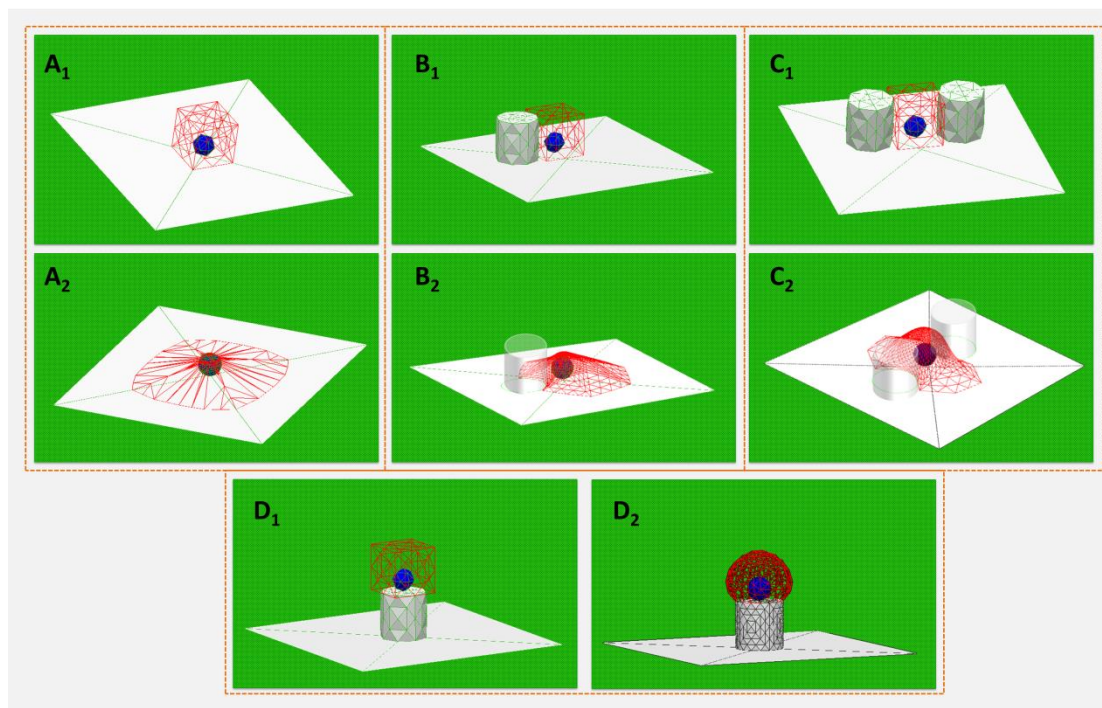


Figure 4. Simulation of individual cell on different substrates. A₁: initial state of cell on the flat surface; A₂: the minimum surface energy state of cell on the flat surface; B₁: initial state of cell beside one pillar; B₂: the minimum surface energy state of cell beside one pillar; C₁: initial state of cell between two pillars; C₂: the minimum surface energy state of cell between two pillars; D₁: initial state of cell on top of one pillar; D₂: the minimum surface energy state of cell on top of one pillar.

3.3 Effects of micropillar topography on cell protein expression

HSCs are the key mediator in progressive liver fibrosis and cirrhosis [30]. The HSCs are dormant under normal conditions, but when the liver is injured, they become active and will generate EMT with decreasing expression of E-cadherin (E-cad) and increasing expression of α -smooth muscle actin (α -SMA). For EMT study, while the diameter and spacing of the micropillars were $5\ \mu\text{m}$ and $2.5\ \mu\text{m}$ [P (5, 2.5)], the micropillar topography could induce significant changes in the expressions of E-cad and α -SMA compared with the flat substrate. In addition, TGF- β , a kind of chemical inducer for inducing EMT, was also used in the study as the positive control. The fluorescence images are shown in Figure 5.

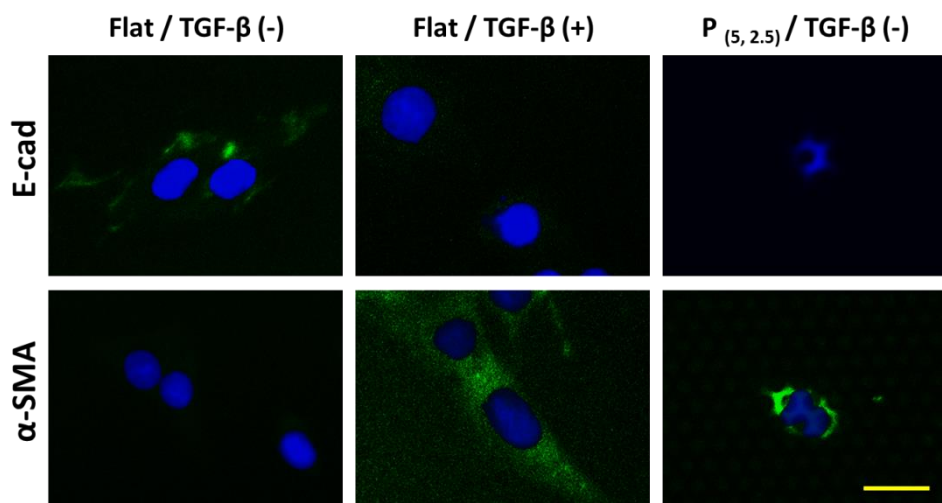


Figure 5. Fluorescence images of the expression of EMT-related proteins with different conditions. E-cad: E-cadherin (Green); α -SMA: α -smooth muscle actin (Green); cell nucleus was stained by DAPI (Blue). Scale bar = 20 μ m.

In physiological conditions, HSCs are located within the micro or sub-micro scale Disse's space, between the parenchymal cells and the sinusoidal endothelial cells of the hepatic lobule [31]. The Disse's space, also called perisinusoidal space, contains the blood plasma and ECM. Some researchers considered that this space to be obliterated in liver disease, especially in liver fibrosis [5]. Hepatic fibrosis was associated with an inflammatory response and deposition of ECM. Following liver injury, HSCs, the main ECM-producing cells, become active and generate EMT with change of cell phenotype and secretion of ECM. A large secretion of ECM would reduce the size of the Disse's space and would most likely further activate the other HSCs, so to aggravate fibrotic liver diseases and may even develop into cirrhosis. We can say that the size of the Disse's space plays an important role in HSCs activation. Notably, it was possible to change the physiological state of the HSCs, so to induce EMT. In our experiment, we found that the expressions of E-cad and α -SMA were changed by a particular size [$P_{(5, 2.5)}$] of the micro pillar, which might be compatible with the size of Disse's space in pathological conditions. In addition, we also found that the cell area of $P_{(5, 2.5)}$ group was the smallest among all groups, because the cell was strictly restricted in the space with highest surface energy. This situation was

probably similar to the cells in the Disse's space full of ECM. The study indicated that the size of established topography might be able to mimic the size of Disse's space in pathological conditions. However, the experimental data like EMT-related gene expression and western blotting is not readily available because of limiting cell number in this study. The change of cell behaviors under this condition calls for further investigation.

4. Conclusions

By localizing the individual hepatic stellate cells in response to the different micropillar topographies, we demonstrated that the morphology of human hepatic stellate cells were greatly associated with the micro pillar topography. As the physical modeling showed, the morphological response of cells to micro pillar topography can be triggered by a minimum interfacial energy. Notably, the established topography with 2.5 μm spacing and 5 μm pillar diameter could affect the expression of E-cadherin and α -smooth muscle actin, and these proteins were closed related to EMT. This unique size might be compatible with the size of Disse's space in real pathological condition. The findings of this study are significant in understanding the mechanisms of liver fibrosis and have potential applications in tissue engineering and therapy.

Acknowledgements

This research was supported by the Special Fund for Agro-scientific Research in the Public Interest, Ministry of Agriculture of the People's Republic of China (No. 201303045), Joint Research Fund of NSFC-RGC (11161160552, N_HKUST601/11), the PhD Start-up Fund of Natural Science Foundation of Guangdong Province and Key Laboratory of Separation Science for Analytical Chemistry, Dalian Institute of Chemical Physics, Chinese Academy of Sciences.

References

1. J. Y. Park, S. Takayama and S. H. Lee, *Integr Biol*, 2010, **2**, 229-240.
2. M. Nikkhah, F. Edalat, S. Manoucheri and A. Khademhosseini, *Biomaterials*, 2012, **33**, 5230-5246.
3. M. P. Lutolf, *Integr Biol*, 2009, **1**, 235-241.
4. L. M. Coussens and Z. Werb, *NATURE*, 2002, **420**, 860-867.
5. R. Bataller and D. A. Brenner, *J. Clin. Invest.*, 2005, **115**, 209-218.
6. W. J. Polacheck, R. Li, S. G. Uzel and R. D. Kamm, *Lab chip*, 2013, **13**, 2252-2267.
7. A. J. Engler, S. Sen, H. L. Sweeney and D. E. Discher, *Cell*, 2006, **126**, 677-689.
8. D. Mitrossilis, J. Fouchard, A. Guirouy, N. Desprat, N. Rodriguez, B. Fabry and A. Asnacios, *P Natl Acad Sci USA*, 2009, **106**, 18243-18248.
9. C. Yu, J. Ma, J. Zhang, J. Lou, D. Wen and Q. Li, *ACS Appl Mater Interfaces*, 2014, **6**, 8199-8207.
10. F. Badique, D. R. Stamov, P. M. Davidson, M. Veuillet, G. Reiter, J. N. Freund, C. M. Franz and K. Anselme, *Biomaterials*, 2013, **34**, 2991-3001.
11. W. T. Su, Y. F. Liao, T. W. Wu, B. J. Wang and Y. Y. Shih, *J Biomed Mater Res A*, 2013, **101**, 185-194.
12. D. Lu, C. Luo, C. Zhang, Z. Li and M. Long, *Biomaterials*, 2014, **35**, 3945-3955.
13. M.-H. Kim, Y. Sawada, M. Taya and M. Kino-oka, *J Biomed Eng*, 2014, **8**.
14. S. Tawfick, M. De Volder, D. Copic, S. J. Park, C. R. Oliver, E. S. Polsen, M. J. Roberts and A. J. Hart, *Adv Mater*, 2012, **24**, 1628-1674.
15. M. Thery, V. Racine, M. Piel, A. Pepin, A. Dimitrov, Y. Chen, J. B. Sibarita and M. Bornens, *P Natl Acad Sci USA*, 2006, **103**, 19771-19776.
16. G. Kumar, C. C. Ho and C. C. Co, *Adv Mater*, 2007, **19**, 1084-1090.
17. G. Mahmud, C. J. Campbell, K. J. M. Bishop, Y. A. Komarova, O. Chaga, S. Soh, S. Huda, K. Kandere-Grzybowska and B. A. Grzybowski, *Nat Phys*, 2009, **5**, 606-612.
18. S. Bauer, J. Park, J. Faltenbacher, S. Berger, K. von der Mark and P. Schmuki, *Integr Biol*, 2009, **1**, 525-532.
19. A. A. Moe, M. Suryana, G. Marcy, S. K. Lim, S. Ankam, J. Z. Goh, J. Jin, B. K. Teo, J. B.

- Law, H. Y. Low, E. L. Goh, M. P. Sheetz and E. K. Yim, *Small*, 2012, **8**, 3050-3061.
20. K. Yang, K. Jung, E. Ko, J. Kim, K. I. Park and S. W. Cho, *ACS Appl Mater Interfaces*, 2013, **5**, 10529-10540.
21. Z. Li, Y. Gong, S. Sun, Y. Du, D. Lu, X. Liu and M. Long, *Biomaterials*, 2013, **34**, 7616-7625.
22. E. K. Yim, S. W. Pang and K. W. Leong, *Exp Cell Res*, 2007, **313**, 1820-1829.
23. S. Ankam, M. Suryana, L. Y. Chan, A. A. Moe, B. K. Teo, J. B. Law, M. P. Sheetz, H. Y. Low and E. K. Yim, *Acta biomater*, 2013, **9**, 4535-4545.
24. M. J. Dalby, N. Gadegaard, R. Tare, A. Andar, M. O. Riehle, P. Herzyk, C. D. Wilkinson and R. O. Oreffo, *Nat Mater*, 2007, **6**, 997-1003.
25. J. Fiedler, B. Ozdemir, J. Bartholoma, A. Plettl, R. E. Brenner and P. Ziemann, *Biomaterials*, 2013, **34**, 8851-8859.
26. Z. Tao, P. Wang, L. Wang, L. Xiao, F. Zhang and J. Na, *J. Mater. Chem. B*, 2014, **2**, 471-476
27. Z. Tao, P. Wang, F. Zhang and J. Na, *BioNanoSci.*, 2014, **4**, 288-300
28. A. Muller, J. Meyer, T. Paumer and T. Pompe, *Soft matter*, 2014, **10**, 2444-2452.
29. Y. Ding, Z. Yang, C. W. Bi, M. Yang, S. L. Xu, X. Lu, N. Huang, P. Huang and Y. Leng, *ACS Appl. Mater. Interfaces*, 2014, **6**, 12062-12070.
30. X. M. Wang, D. M. Yu, G. W. McCaughan and M. D. Gorrell, *Hepatology*, 2005, **42**, 935-945.
31. H. Senoo, *Med Electron Microsc*, 2004, **37**, 3-15.